A spin–orbit playground: surfaces and interfaces of transition metal oxides

Gariglio, Stefano; Caviglia, Andrea; Triscone, Jean-Marc; Gabay, M

How to cite

GARIGLIO, Stefano et al. A spin–orbit playground: surfaces and interfaces of transition metal oxides. In: Reports on Progress in Physics, 2019, vol. 82, n° 012501. doi: 10.1088/1361-6633/aad6ab

This publication URL: https://archive-ouverte.unige.ch/unige:114085
Publication DOI: 10.1088/1361-6633/aad6ab

A Spin-Orbit Playground: Surfaces and Interfaces of Transition Metal Oxides

S Gariglio[1], A D Caviglia[2], J-M Triscone[1], M Gabay[3]

[1] DQMP, University of Geneva, 24 Quai E.-Ansermet 1211 Geneva, Switzerland
[2] Kavli Institute of Nanoscience, Delft University of Technology, Delft, The Netherlands
[3] Laboratoire de Physique des Solides, Université Paris-Sud, Bâtiment 510,91405 Orsay Cedex, France

E-mail: `stefano.gariglio@unige.ch`

Abstract. Within the last twenty years, the status of the spin-orbit interaction has evolved from that of a simple atomic contribution to a key effect that modifies the electronic band structure of materials. It is regarded as one of the basic ingredients for spintronics, locking together charge and spin degrees of freedom and recently it is instrumental in promoting a new class of compounds, the topological insulators. In this review, we present the current status of the research on the spin-orbit coupling in transition metal oxides, discussing the case of two semiconducting compounds, $SrTiO_3$ and $KTaO_3$, and the properties of surface and interfaces based on these. We conclude with the investigation of topological effects predicted to occur in different complex oxides.

Submitted to: *Rep. Prog. Phys.*

1. Introduction

The spin-orbit interaction is a relativistic effect that couples the angular momentum of an electron with its spin. In a qualitative description, the electric field $\mathbf{E}$ generated by the atomic nucleus is seen by a moving charge as an effective magnetic field $\mathbf{B_{eff}} = -(\mathbf{v}/c) \times \mathbf{E}$; for an electron with a magnetic moment $\mathbf{m}$ (given by its spin $\mathbf{S}$), it results in an interaction between $\mathbf{B_{eff}}$ and $\mathbf{m}$ that can be expressed with a Hamiltonian term of the form $H_{ASO} = -\mathbf{m} \cdot \mathbf{B_{eff}}$. After some algebra, this term can be written as $H_{ASO} = \lambda \mathbf{L} \cdot \mathbf{S}$ [1]. This is the atomic spin-orbit interaction and this simple description provides an estimate that turns out to be a factor of two larger than what is measured experimentally. The spin-obit interaction explains the fine structure of the atomic emission lines, which provide a unique signature of the different elements. The coupling constant λ reflects the strength of the atomic electric field and varies with the number of protons Z as Z^2, with a complex, shell-dependent scaling for the outermost electrons when screening from valence electrons is taken into account [2], whereas it would change as Z^4 in a hydrogen-like approximation that neglects the screening of the nuclear potential provided by the core electrons [3, 4].

The standard description of an electron in a solid considers its interaction with its environment (the lattice and the other electrons) with a degree of relevance proportional to the interaction strength. If, for instance, we look at the Hamiltonian H for electrons of $3d$ ions in a crystal, it is usually factorized as: $H = H_I + H_L + H_{SO} + H_{JT}$ where H_I is the free ion Hamiltonian without the spin-orbit coupling, H_L is the interaction with the periodic static lattice potential, H_{SO} is the spin-orbit coupling (SOC) term and H_{JT} characterizes the interaction of the electron with the crystal lattice vibrations. The atomic spin-orbit coupling becomes a correction, since the energy scales of the different terms are approximatively 1-10 eV for H_I and H_L, 0.01-1 eV for H_{SO} and H_{JT}. An important differences between these terms is that while the H_I, H_L and H_{JT} Hamiltonians mix states with the same spin, the spin-orbit interaction mixes states with different spins. This is due to the fact that the former three interactions result from the Coulomb force and do not act on the spin channel.

The effect of the SOC on the electronic states is to split the energy levels of orbitally degenerate states, lifting the degeneracy similarly to the fine structure of an atom. For many materials, this energy splitting is small in comparison to the one induced by structural distortions; it is however important for t_{2g} electronic states of $3d$ ions in octahedral coordination in cubic structures ($SrTiO_3$, $KTaO_3$) or for $2p$ states of IV elements (Si, Ge,..) in tetragonal coordination with diamond structure. The consequences are felt more strongly close to the top or bottom of a band where the states are degenerate while are usually negligleable elsewhere due to the band dispersions. Figure 1 illustrates the SOC effect on the top of the valence band of a semiconductor with a direct gap (E_g). Since the spin-orbit interaction couples spin and orbital angular momentum, the electronic states are defined by their total angular momentum: for these p-like valence band edge states, the quantum numbers are j=3/2 (heavy and light hole

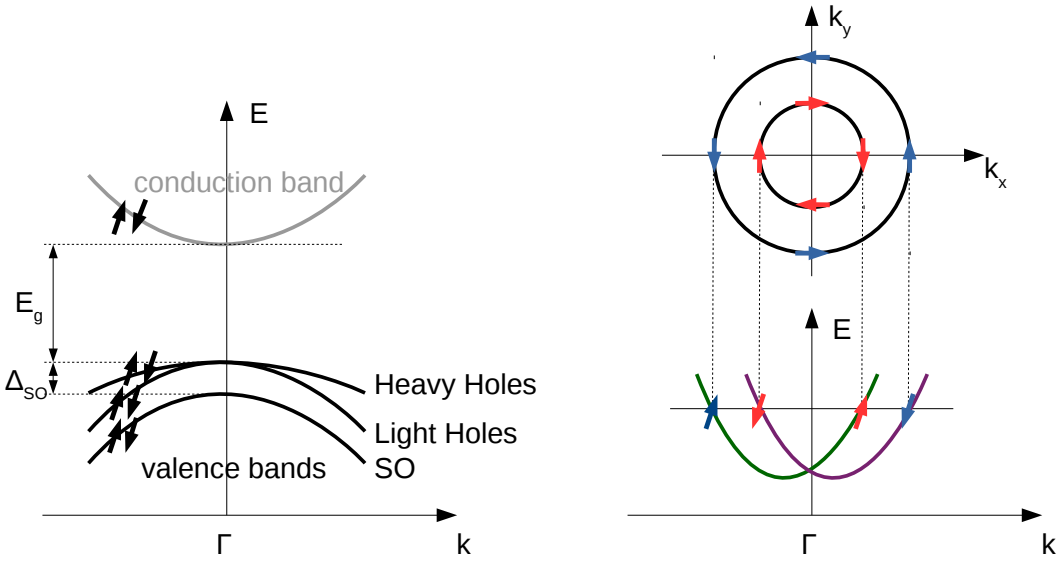

Figure 1. Left: The sketch illustrates the effect of the spin-orbit interaction on the band structure of a semiconductor close to the fundamental gap E_g, leading to the spin-orbit gap Δ_{SO} separating the j=3/2 (heavy and light hole bands) from the j=1/2 split-off (SO) band. The bands are spin-degenerate. Right: Schematics of the band dispersion in presence of breaking of inversion symmetry, which removes the spin degeneracy and (top) view of the spin pattern on the Fermi surface.

bands) and j=1/2 (split-off SO band) and these states are split by an energy gap Δ_{SO}, which is called the spin-orbit gap.

The effects of SOC have been studied intensively in semiconductors, where the energy scales of the Fermi level and of the spin-orbit gap are comparable [5]. For semiconductor-like complex oxides as $SrTiO_3$, electronic band structure calculations revealed that the effect of SOC is dominant with respect to the energy changes induced by low temperature structural (tetragonal) distortions. For semiconducting compounds with heavier transition metal ions like $KTaO_3$, the SOC gap becomes important (400 meV) and affects strongly the band structure at the conduction band edge. We will review experimental and theoretical work on semiconductor oxides in Section 2.

In recent years, research on SOC in transition metal oxides has turned to materials of the 4*d* and the 5*d* series where the spin-orbit gap Δ_{SO} becomes comparable to the on-site Hubbard repulsion U [6, 7, 8]. For these materials, epitomized by the iridate compounds, the competition between electron hopping (i.e. bandwidth), electron-electron correlation and SOC gives rise to complex phase diagrams with conducting and insulating states (Mott/Axion/Topological insulators) and magnetic orders. A description of the physics of these systems has been recently reviewed in several references [6, 7, 8, 9]: we address the reader to that literature.

The spin-orbit coupling occurs whenever a charged particle moves in an electric field. The general expression of this effect is given by the Hamiltonian: $H_{SO} = (\hbar^2/2m^2c^2)(\boldsymbol{\nabla} V \times \boldsymbol{k}) \cdot \boldsymbol{\sigma}$ where $\boldsymbol{\nabla} V$ is the potential gradient, $\boldsymbol{k}$ the particle momentum and $\boldsymbol{\sigma}$ its spin. In a solid, beyond the electric fields of the nuclei as discussed before,

local electric fields can exist due to the breaking of inversion symmetry in the crystal structure or due to the presence of an asymmetric confining potential in quantum wells. In these cases, since the potential seen by the carriers breaks the inversion symmetry, the spin degeneracy is removed and two branches for the energy dispersion $E_+(\mathbf{k})$ and $E_-(\mathbf{k})$ appear. The right panel in Figure 1 illustrates the energy dispersion for the two branches. When the breaking of inversion symmetry is due to the crystal structure, like in the zinc blend structure of GaAs or InSb, the SOC is of the Dresselhaus type [10, 11]; when it is due to the confinement potential in a quantum well with a polar axis, it is referred as Rashba SOC [12, 13].

In both cases, the SOC entangles the momentum and spin of the electron, locking these two degrees of freedom together. This leads to a number of intriguing phenomena, particularly in transport [14], enabling the manipulation of spin states through charge currents or the inverse effect, a possible realisation of the "spintronics" paradigm [15]. Recently, it is at the surface or at the interface of heterostructures containing heavy elements like Au or Bi (the atomic SOC boosts the inversion asymmetry SOC) that spin-polarized surface states have been observed [16, 17](see [18] for a recent review on the subject) and topological properties have been uncovered [19].

The study of inversion asymmetry SOC is relatively new in oxide heterostructures. In this review we will present the current status of research with particular focus to the experimental results in $SrTiO_3$-based systems and theoretical predictions for transition metal oxide surface and heterostructures. A final section will be devoted to the calculations of topological effects in these systems.

2. SOC in $SrTiO_3$ and $KTaO_3$: bulk, surface and interfaces

2.1. Bulk $SrTiO_3$

Between the family of complex oxides with perovskite structure (see Figure 2), $SrTiO_3$ stands as a remarkable example of the variety of properties these materials can display. In its stoichiometric form, it is an incipient ferroelectric, i.e. quantum fluctuations suppress the formation of a long-range ferroelectric ground state [20] which can be induced by substituting ^{16}O with ^{18}O [21] or Sr with Ca [22]. Electron doping by replacing Sr with La, Ti with Nb or introducing oxygen vacancies produces a semiconductor with a high carrier mobility and, in a certain doping range, a superconducting ground state [23]. The insulator-metal transition occurs at an extremely low carrier density, $\sim 10^{16}\,\mathrm{cm}^{-3}$, for which the Fermi level lies few meV above the bottom of the conduction band. This occurs at the Γ point where the electronic structure displays three spin-degenerate bands, formed by d_{xy}, d_{xz} and d_{yz} orbitals of Ti t_{2g} states slightly hybridized with O $2p$ states, that are split by the Ti $3d$ spin-orbit coupling (Δ_{SO}) and, at low temperature, by the tetragonal distortion (Δ_z). The effect of these two energy terms was first calculated by Mattheiss [24] and is shown in the right panel of Figure 2: we observe that the spin-orbit splitting present in the cubic structure

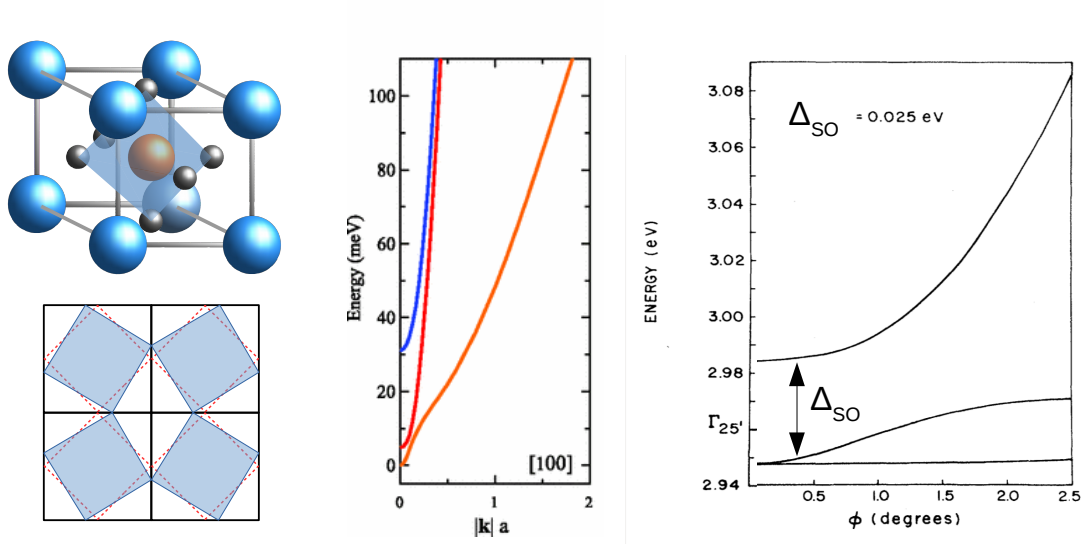

Figure 2. Left: Top: Unit cell of $SrTiO_3$ in its room temperature cubic form. At low temperature (bottom), the oxygen octahedron rotates about the vertical axis: a view of the TiO_2 (0 0 1) plane along the [0 0 1] direction shows the octahedra (continuous blue lines) in the tetragonal structure rotated by an angle ϕ with respect to the high temperature position (dashed red lines). Centre: Band dispersion for the [100] direction of the low-temperature tetragonal phase: the splittings at the Γ point between the bands with different dispersion is due to the spin-orbit coupling (which lifts the blue band) and the tetragonal crystal field (separating the red and orange bands). Reprinted with permission from D. van der Marel *et al.*, Phys. Rev. B **84**, 205111(2011) Copyright (2011) by the American Physical Society. Right: evolution of the conduction band minima as a function of the rotation angle ϕ calculated using an atomic spin-orbit parameter for Ti of $\Delta_{SO} = 25$ meV. Reprinted with permission from L. Mattheiss, Phys. Rev. B **6**, 4740 (1972). Copyright (1972) by the American Physical Society.

(ϕ=0, being ϕ the rotation angle of the oxygen octahedron about the vertical axis of the tetragonal unit cell) mixes with the distortion splitting as ϕ increases to reach its low temperature value of $\sim$2.2°.

More recently, first principle methods have been employed to determine the electronic structure of the distorted structure [25, 26]. The center panel of Figure 2 shows the dispersion of the conduction bands close to the Γ point for a momentum along the [1 0 0] crystallographic direction: we note an atomic spin-orbit splitting of 19 meV and a crystal field splitting due to the tetragonal distortion of 4 meV [25]. With the purpose to describe more precisely the bottom of the conduction band, the $\mathbf{k} \cdot \mathbf{p}$ method as well as a band edge effective Hamiltonian have been developed [27, 28]; these theoretical descriptions allow one to extract accurate parameters from experiments. Based on such theoretical framework, the analysis done by Allen and co-workers on Shubnikov-de Haas oscillations for samples with Fermi level in the spin-orbit gap has confirmed the small value of the tetragonal crystal field splitting ($\Delta_z \sim 2$ meV), in line with previous experimental estimates [29, 30]; a value of the spin-orbit splitting could not, however, be provided. An experimental confirmation of the detailed structure of

the bottom of the conduction band of $SrTiO_3$ is currently still missing. One difficulty is that techniques like angle-resolved photoemission electron spectroscopy are surface sensitive and hence probe a different state induced by breaking of inversion symmetry and band bending effects occurring at the surface of the material (see next section).

2.2. $SrTiO_3$-based interfaces

2.2.1. The experiments The first experiments to reveal the presence of spin-orbit coupling at $SrTiO_3$-based interfaces have been magneto-transport measurements performed at low temperatures. Several groups were investigating the interface between $LaAlO_3$ and $SrTiO_3$ that was discovered to host a quasi-2D electron liquid in 2004 [31] and, few years later, to become superconducting below 300 mK [32] (a review of the system is presented in Ref. [33] and a more broad survey on $SrTiO_3$-based heterostructures is discussed in Ref. [34]). Probing the superconducting state in field effect devices, Ben Shalom and co-workers observed that the critical magnetic field, when applied parallel to the 2D superconducting layer, exceeds the Pauli paramagnetic limit, i.e. the coupling strength of a Cooper pair [35]. They related the excess of magnetic field to the presence of a strong spin-orbit interaction. Remarkably, they also observed that the strength of the spin-orbit coupling could be varied by the gate voltage. Studying the magnetotransport in the normal state on similar field effect devices, weak-anti-localisation corrections to the conductance were observed [36]. In panels (a) and (b) of Figure 3 are shown the magneto-conductance curves revealing the transition from weak-localisation (positive magneto-conductance) to weak-anti-localisation (negative magneo-conductance) conduction as the gate voltage is increased. From the analysis of the data, the spin-orbit coupling constant reveals a strong dependence on the gate voltage, as shown in Figure 3(c). To probe the type of spin-orbit coupling these authors have looked at the relation between the elastic and the spin-orbit scattering times. This approach allows one to distinguish between an atomic spin-orbit interaction (where a direct proportional relation between the two scattering times is expected according to the Elliot-Yafet mechanism [37, 38]) and a spin-orbit interaction originating from a breaking of inversion symmetry (where the relation between the two scattering times in inversely proportional as described by the D'ykanov-Perel' mechanism [39]). They verified the consistency of the results with the D'ykanov-Perel' mechanism, implying that the nature of the spin-orbit coupling is of Rashba type. We note that the strength of the spin-orbit coupling, of the order of few meV, is on the same scale as the energy of the Fermi level. Both groups were relating the occurrence of the Rashba interaction to the breaking of the inversion symmetry of the system and the presence of the electric field that confines the electron liquid at the interface: in this picture, its modulation with a gate voltage stems from the modulation of the electric field at the interface.

The relation between the orbital structure and the modulation of the spin-orbit interaction at the $LaAlO_3/SrTiO_3$ interface was originally investigated by Joshua and co-workers [40]. Analysing the evolution of the longitudinal and transverse (Hall) resistance

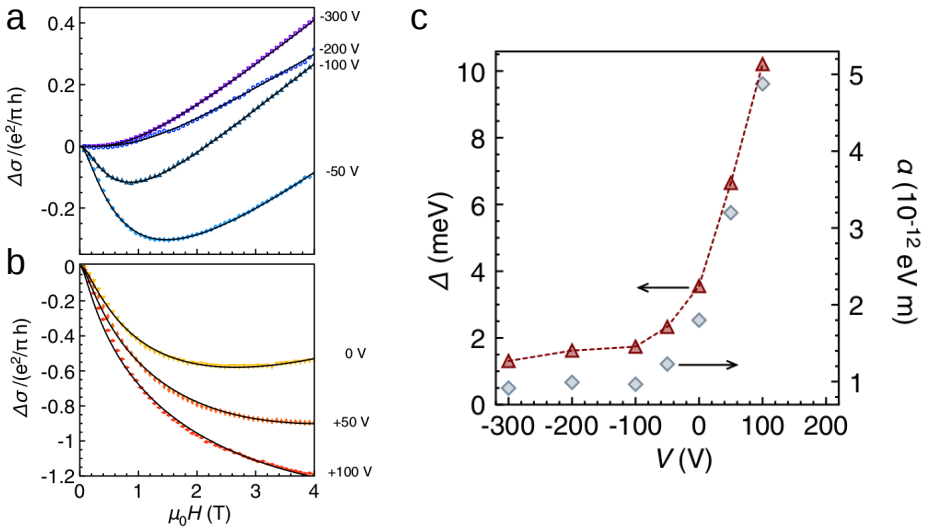

Figure 3. a and b: Magneto-conductance curves for several gate voltages with best fits according to the Maekawa-Fukuyama theory describing spin-orbit weak anti-localisation behaviour. c: Evolution of the spin splitting energy Δ vs gate voltage as extracted from the fits of the magneto-conductance. Reprinted with permission from A. Caviglia *et al.*, Phys. Rev. Lett. **104**, 126803 (2010). Copyright (2010) by the American Physical Society.

in magnetic field for different doping levels induced by gate tuning, they uncovered a critical carrier density signaling a transition from single to multiple band transport. This value, universal in their description, marks a Lifshitz transition and the initial filling of the hybridized d_{xz}/d_{yz} band whose bottom lies 50 meV above the bottom of the d_{xy} band (see Figure 4). At slightly higher energy, these two bands cross in k-space due to their different dispersion: due to the atomic spin-orbit coupling, however, these crossing points are avoided since a new hybridization between the states occurs that lifts the degeneracy. This particular band configuration leads to an effective spin-orbit coupling whose strength depends strongly on the doping level, as shown in Figure 4c. The effective SOC strength varies also in the k-space, being larger at the avoided crossing k points and smaller elsewhere. In combination with the Rashba SOC this produces a spin splitting at the avoided level crossing that is much larger than the one present at the zone centre. An effective tight-binding hamiltonian modelling this electronic structure and its spin texture was proposed by Diez *et al.* [41, 42]

In this picture, the Rashba SOC component due to the breaking of inversion symmetry adds on top of this effect but is small. This new scenario questions the coupling of the spin to the momentum.

The spin texture on the Fermi surface is indeed particularly relevant with respect to the superconducting condensate and to spin transport in the electron liquid. Nakamura *et al.* suggested that the Rashba spin-orbit coupling is cubic in momentum k and not linear. For a linear in k SOC one expects that the electron spin rotates around the Fermi surface to remain perpendicular to $\boldsymbol{k}$, as shown in the left panel of Figure 5, but

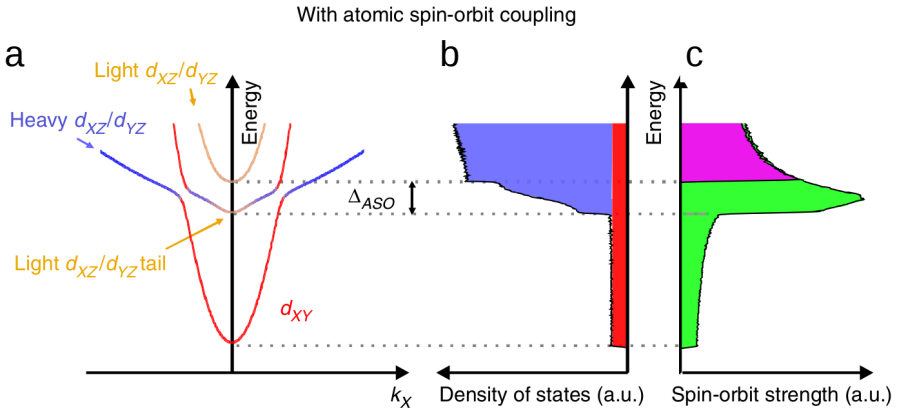

Figure 4. a: Band dispersion along the [1 0 0] direction (k_x) revealing the avoided crossings between the light d_{xy} band and the heavy d_{xz}/d_{yz} band. We see that when the Fermi level starts to fill the bottom of the heavy band, a large increase in the density of states (b) occurs with a parallel increase of the spin-orbit coupling strength (c). At the avoided crossing, the SOC peaks and then decreases, in agreement with the experimental reports of Caviglia [36] and Ben Shalom [35]. Reprinted by permission from Nature, A. Joshua *et al.*, Nat. Commun. **3** 1129 (2012), Copyright (2012).

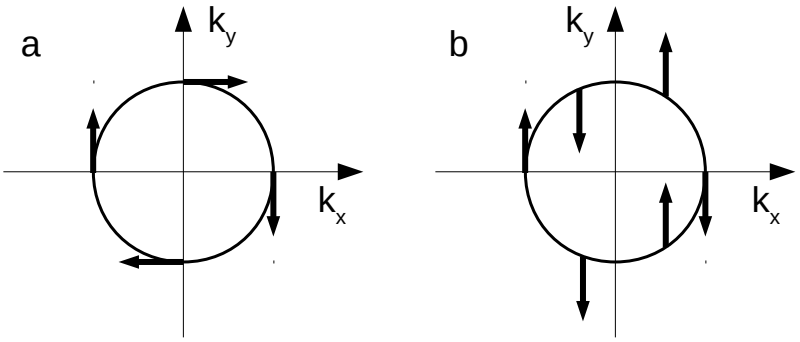

Figure 5. a): Spin texture on one of the Fermi surfaces of the spin-split d bands for the case of linear in k Rashba SOC. b): For a cubic in k Rashba SOC, the spin rotates faster around the Fermi surface. Reprinted with permission from H. Nakamura *et al.*, Phys. Rev. Lett. **108**, 206601 (2012). Copyright (2012) by the American Physical Society.

in cubic in k SOC the spin rotates faster around the Fermi surface as shown in the right panel [43].

One way to probe the coupling between spin and momentum is via the Rashba-Edelstein effect and its inverse. In presence of Rashba spin-orbit interaction, injecting a charge (spin, for the inverse effect) current into the material creates an imbalance of spin (charge). Experiments performed by Lesne and coworkers and Chauleau and coworkers using the inverse mechanism have revealed a charge current when a spin current was injected by tunneling from a magnetic layer [44, 45]. They have also shown that the dependence upon gate voltage of the SOC strength follows the prediction for the scenario

of avoided crossings, i.e. the coupling first increases and then decreases for increasing band filling. The particular angular dependence observed by Chauleau *et al.* for the intensity of SOC strongly reminds the prediction of the dependence on the $\boldsymbol{k}$ vector of the spin-splitting on the Fermi surface passing trough the avoided crossings (see panel (e) in Figure 6).

These experiments, confirming the Rashba SOC effects in combination with orbital splitting, show the potential of this electron liquid for spintronics applications due to its strong tunability with a gate voltage.

2.2.2. The theory For bulk $SrTiO_3$ we have seen that the atomic spin-orbit coupling is of the order of 10-20 meV and manifests prominently at the degenerate Γ point. For the interface, the quantum confinement of the electrons lowers the energy of the d_{xy} states, leading to a degeneracy at four separate k points with the hybridized d_{xz}/d_{yz} states. When the crossings between these bands occur, the atomic spin-orbit coupling hybridizes all these states, leading to a new entanglement between the orbital and spin degrees of freedom: this picture explains the strong SOC and its large modulation with gate voltage observed in experiments. Figure 6 illustrates the differences between the electronic bands in bulk $SrTiO_3$ and at the interface, the role of atomic spin-orbit and the effects of the breaking of inversion symmetry, according to density-functional-theory (DFT) calculations [46]. In panel (a) is shown the band dispersion for bulk $SrTiO_3$ with and without atomic SOC: we see its effect at the Γ point where it lifts the degeneracy and hybridizes the $d_{xy}/d_{xz}/d_{yz}$ states into new states with Γ_8^+ and Γ_7^+ symmetry and different effective masses. For the interface, the quantum confinement of the electrons changes the band order: Figure 6(b) displays the novel configuration with an interface induced splitting between the d_{xy} and d_{xz}/d_{yz} bands at the Γ point of $\sim$300 meV. The role of the spin-orbit coupling is evident when two bands cross or coincide, as calculations without (dashed black line) and with (red-blue continuous lines) SOC show. Figure 6(e) displays the amplitude of the spin-splitting at two different Fermi levels resulting from these calculations. The graph plots the amplitude around the Fermi surface for a Fermi level lying close to the bottom of the d_{xy} band (green line) where only Rashba SOC is present and at the avoided crossings (brown line) where both atomic and Rashba SOC occur. Beside the large difference in value, we note the strong dependence on k when we reach the avoided crossings.

A description of the system with a tight-binding model introduces the breaking of inversion symmetry as an antisymmetric (it changes sign with hopping direction) hopping term, usually forbidden in bulk for symmetry arguments, between states of different symmetries. For the interface, the study by Khalsa and co-workers [47] shows that the electric field polarizes the $SrTiO_3$ lattice, displacing the Ti and O atoms in opposite directions. This deformation allows a new hopping term between d_{xy} and d_{yz} or d_{xz}, whose amplitude is then proportional to the electric field, thus recovering the Rashba interaction. In this way, the tight-binding model maps the DFT results.

Considering the complexity of the Fermi surface of the electron liquid presented

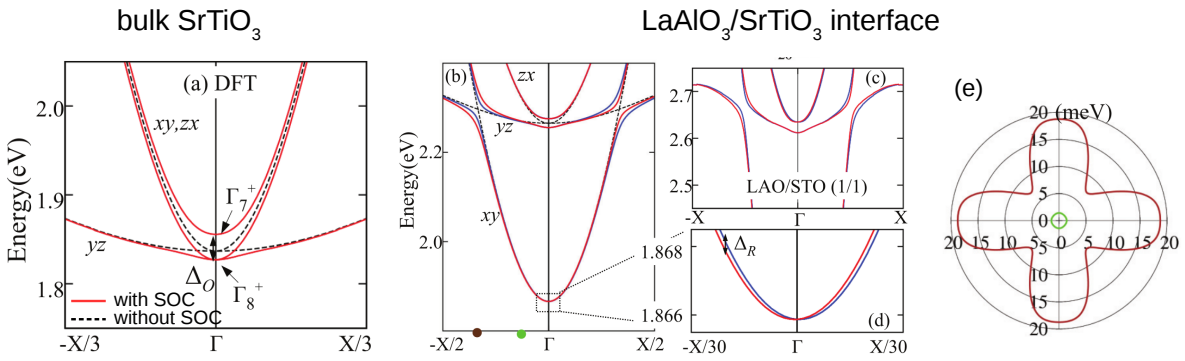

Figure 6. (a) Band structure of bulk $SrTiO_3$ obtained by DFT calculation without and with SOC. (b) Band dispersion for the $LaAlO_3/SrTiO_3$ interface without (dashed line) and with (continuous lines) SOC and breaking of inversion symmetry. The blue and red colors differentiate the spin state. Zoom of the crossing region (c) and of the bottom of the band (d) with the spin-spitting Δ_R induced by the breaking of inversion symmetry (Rashba SOC). (e) Angular dependence of the spin splitting at the bottom of the d_{xy} band (green line referring to the green point in (b)) where it is Rashba SOC and at the $d_{xy} - d_{yz}/d_{zx}$ crossing region (brown). Reprinted with permission from Z. Zhong *et al.*, Phys. Rev. B **87**, 161102 (2013). Copyright (2013) by the American Physical Society.

above, naturally arises the question on the origin and symmetry of the superconducting state. For a single d_{xy} band split by Rasba SOC, Yada and coworkers find that the pairing function consists of a mix of spin-singlet ($\uparrow\downarrow$) even-parity (d_{xy}-wave) pairing and spin-triplet ($\uparrow\uparrow$ or $\downarrow\downarrow$) odd-parity ($p_x \pm ip_y$-wave) pairing, with a ratio that varies with the carrier density [48]. In this study, the origin of the pairing was assumed to be the strong electron correlations of the Ti $3d$ electrons. Allowing both electron-phonon (e-ph) and electron-electron (e-e) coupling and considering two bands with SOC, the pairing function calculated by Scheurer and Schmalian [49] can be that of a topologically trivial or non-trivial superconducting state. For e-ph coupling, being the sign of the order parameter the same on the two Fermi surfaces, the superconducting state is topologically trivial. In case of e-e coupling, the order parameter changes sign between the two Fermi surfaces and the superconducting state becomes topologically non-trivial, i.e. the transition from a trivial BCS state into this state requires the closing of the gap on one of the Fermi surfaces. One way to probe the symmetry and hence the origin of the superconducting state would be to look at the sensitivity of the critical temperature on impurity scattering [50].

2.3. The $SrTiO_3$ surface

Beyond the observation of a 2D electron liquid at the interface between $LaAlO_3$ and $SrTiO_3$, Santander *et al.* [51, 52] using Angular Resolved Photoemission Spectroscopy (ARPES) evidenced the existence of a nanometer thin conducting layer at the bare surface of (001)-oriented $SrTiO_3$ cleaved in high vacuum. Its carrier concentration was

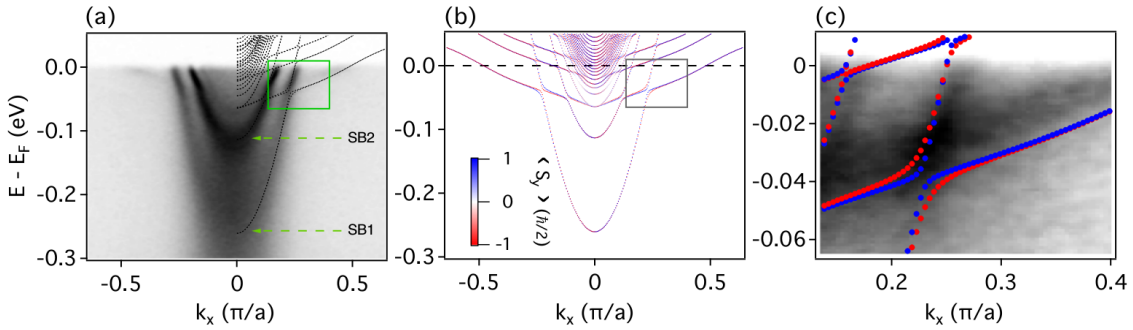

Figure 7. ARPES rusults and band structure calculations of the subband structure of (001) $SrTiO_3$ surface. (a) Energy dispersion measured by high-resolution ARPES taken with *s*-polarized light along the [100] direction with over-plotted tight-binding calculations (black dashed lines). (b) Calculations of the subbands resolved in spin. (c) Zoom on the avoided crossing region (green box in panel (a)), measured with *p*-polarized light to reveal the heavy subband. Reprinted with permission from S. McKeown Walker *et al.*, Phys. Rev. B **93**, 245143 (2016). Copyright (2016) by the American Physical Society.

estimated around $10^{14}\,\mathrm{cm}^{-2}$ and the orbital character of the electronic bands was quite consistent with that found for the $LaAlO_3/SrTiO_3$ interface, the lowest having a d_{xy} symmetry and the higher ones, close to E_F, having $d_{xz/dyz}$ symmetry (see Figure 7). An ubiquitous in-gap state positioned at 1.3 eV below E_F and the pull-down of the valence band led the authors to ascribe the origin of the 2D electron liquid to oxygen vacancies confined near the surface. These are formed when illuminating the sample with the UV light of the beam. The orbital character of the bands is explained by three main factors. One is the kinetic energy of the carriers along the direction of the surface (of order 230 meV at E_F). Two is the bulk spin-orbit energy (30 - 35 meV) which produces coherent combinations of t_{2g} and spin states. Three is the confining potential (estimated to be 260 meV) which gives a lower energy for the d_{xy} band. Since the spin-orbit energy is one order of magnitude less than the other two, one finds essentially pure d_{xy}, $d_{xz/yz}$ characters except close to the Γ point and to the avoided crossing points of the light (d_{xy}) and heavy ($d_{xz/yz}$) bands.

Subsequently, spin-resolved ARPES measurements (S-ARPES) highlighted the existence of spin winding of the light (d_{xy}) bands at E_F [53] (see Figure 8). Based on the analysis of the data it was concluded that the Rashba spin-orbit energy was on the order of 10 meV. There was some debate about the linear versus cubic nature of the effect, but it was suggested by Baumberger *et al.* [54, 55] that the size and momentum dependence of the surface spin-orbit term can be tied to the proximity of E_F to avoided crossing points of the heavy and light bands. Surface rumpling and atomic displacements imply that the d_{xz}/d_{yz} orbitals now have a finite, oxygen mediated, overlap with the d_{xy} orbitals [46, 47]. Adding the corresponding contribution to the kinetic and spin-orbit terms in the Hamiltonian produces a Rashba-like energy. The strength of the mixing

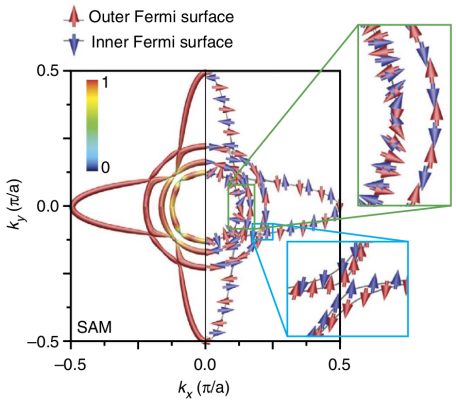

Figure 8. Calculated Fermi surface of the (001) $SrTiO_3$ surface showing the magnitude (left, in units of $\hbar/2$) and direction (right) of the spin. These calculations expose the spin angular momentum-kinetic momentum locking occurring at the Fermi surface for the different orbitals. For the circular d_{xy} subbbands, we observe that the spins wind tangentially to the Fermi contour (i.e. the spins are aligned perpendicularly to the kinetic momentum), while for the elliptical d_{xz}/d_{yz} subbands they are aligned almost perpendicular to the Fermi contour (i.e. the spins are aligned perpendicularly to the dominant contribution of the kinetic momentum, k_y for the d_{yz} and k_x for the d_{xz}). At the avoided crossing points (see the enlargement at the bottom right square), each subband splits for the two spin states, resulting in an effective Rashba-type spin-orbit interaction. Reprinted by permission from Nature, P. King *et al.*, Nat. Commun. **5** 3414 (2014), Copyright (2014).

effect depends on the energy difference between the heavy and light bands so it becomes less and less pronounced as one moves away from the avoided crossing points. *Ab-initio* calculations have been performed on $SrTiO_3$ slabs in the presence of vacancies [56, 57]. For apical divacancy configurations, Altmeyer *et al.* found quantitative agreement with the S-ARPES results and furthermore highlighted the existence of localized magnetic states of e_g character in the vicinity of Ti sites positioned at the center of octaedra with divacancies. Similarly to what is found at the gate controlled $LaAlO_3/SrTiO_3$ interface, fingerprints of Rashba SOI are expected when performing transport measurements: at temperatures on the order of 1-2 K a positive magnetoresistance should be seen as a consequence of weak antilocalization physics. By capping $SrTiO_3$ with a 2 Å thin Al layer, Rödel *et al.* were able to create a fairly homogeneous distribution of vacancies at the surface and at the same time to protect it against re-oxygenation when performing transport experiments in a back-gate geometry [58, 59]. They reported variations of the magnetoresistance with the gate, mobilities (1000 cm^2/Vs) and carrier concentrations ($10^{12}\,cm^{-2}$) reminding of their $LaAlO_3/SrTiO_3$ counterpart. Similar values are found when creating vacancies at the surface of STO through Ar^+ ionic bombardment albeit with larger values of the carrier numbers [60].

An alternative route to creating a 2D electron liquid at the surface of $SrTiO_3$ is through (top-gate) electrostatic doping. An electric-double-layer (EDL) field-effect transistor (FET) setup was used by Ueno *et al.* [61, 62]. In order to avoid contamination

of the surface by chemicals, Gallagher *et al.* [63] introduced a sub-nanometer thin BN buffer layer allowing them to reach mobilities on the order of $10^4\,\mathrm{cm}^2/\mathrm{Vs}$, carrier concentrations of about $10^{14}\,\mathrm{cm}^{-2}$ and exhibiting positive magnetoresistances. Nakamura *et al.* [43] made use of a parylene top-gate to produce a 2D electron liquid at the surface of $SrTiO_3$. Their analysis of magnetotransport led them to advocate a cubic Rashba term as the cause of the observed weak antilocalization behavior with a strength of about 0.5 meV, one order of magnitude less than reported in the above measurements. The low value of the carrier concentration ($3\text{-}8\times10^{12}\,\mathrm{cm}^{-2}$) could explain both the cubic-like term and the discrepancy in the determination of its size [55]. The tunability of the Rashba contribution as well as its magnitude allows one to envisage spintronic applications, exploiting for example the so-called inverse Edelstein effect [44].

2.4. $KTaO_3$

$SrTiO_3$ is not the only perovskite where a 2D electron liquid has been evidenced at bare surfaces. Nakamura *et al.* [64] achieved electrostatic doping at the surface of (001) oriented potassium tantalate, $KTaO_3$, crystal, indicative of a conducting sheet. Subsequently, by fracturing a $KTaO_3$ crystal along the (001) plane in ultra high vacuum, a nanometer thin conducting sheet was revealed in ARPES measurements [65, 66]. The significance of these findings pertains to the spin-orbit energy that one has for carriers in the 2D electron liquid. Since Ta is a $5d$ element, one expects a much higher bulk spin-orbit energy for $KTaO_3$ than for $SrTiO_3$, where Ti is a $3d$ element. As mentioned before, SOI increases as Z^2, where Z is the charge number of the element. Indeed, E_{SO}=400 - 450 meV for $KTaO_3$ versus 30 - 35 meV for $SrTiO_3$. Furthermore a naive charge counting suggests that KO layers carry a negative charge and TaO_2 a positive charge. Hence, in the absence of surface reconstructions, the surface is polar and prone to a polar catastrophe scenario, even in the absence of oxygen vacancies. This consideration may help explain the larger values of the confining potential for $KTaO_3$ (550 meV). This corresponds to an a mean electric field $F_{KTO} = 250\,\mathrm{MV/m}$ as opposed to $F_{STO} = 80\,\mathrm{MV/m}$ for $SrTiO_3$. For $KTaO_3$, E_F (= 400 meV) is of the same order as the spin orbit and confining energies. Accordingly, the orbital character of the bands encodes the spin-orbital locking up to the Fermi energy. The effective mass of the lowest band is about $0.3\,m_e$ and that of the second, higher energy, band of about $1\,m_e$. Given the magnitude of E_{SO} and F_{KTO}, one would have expected a much larger value of the Rashba surface SOI than in the case of $SrTiO_3$. Surprisingly the momentum shift that accompanies it is found in ARPES to be of at most $0.01\,\text{Å}^{-1}$ in $KTaO_3$, ten times less than for $SrTiO_3$ [65]. A puzzling feature is that the estimated carrier concentration at E_F is about the same ($\sim 1.4\times10^{14}\,\mathrm{cm}^{-2}$) as in $SrTiO_3$. An estimate of the Rashba contribution for $KTaO_3$ can be extracted from the magnetoresistance analysis of Nakamura and Kimura [64] based on a cubic Rashba scenario. The carrier concentration n_{2D} in their samples is of order $3\times10^{12}\,\mathrm{cm}^{-2}$, and the spin-orbit diffusion length for the highest gate voltage is l_{SO}=20 nm. With a carrier mass of $\sim 1\,m_e$, one

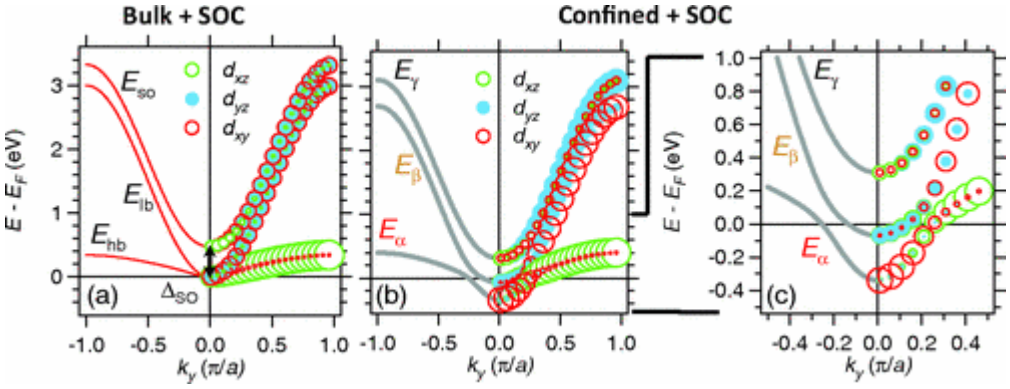

Figure 9. Tight-binding calculations for $KTaO_3$ bulk with spin-orbit coupling (SOC) and surface with SOC (Confined + SOC). The weight of the d_{xz}, d_{yz} and d_{xy} orbital symmetry in each band/subband is proportional to the size of the circles. Reprinted with permission from A. Santander-Syro *et al.*, Phys. Rev. B **86**, 121107 (2012). Copyright (2012) by the American Physical Society.

has

$$\Delta_{SO} = \frac{2\pi\hbar^2\sqrt{n_{2D}}}{\sqrt{2}l_{SO}m_e} \sim 3\,\text{meV}$$

This value is one order of magnitude larger than what Nakamura and Kimura [43] found for $SrTiO_3$ but it falls within the range of what is found for $LaAlO_3/SrTiO_3$. If confirmed, that might make $KTaO_3$ perhaps less appealing than one might have expected *a priori* for spintronics. We note that the DFT calculation performed by Shanavas and Satpathy [67] yields a linear Rashba contribution of about 0.3 eVÅ for the surface of $KTaO_3$. If we use an ARPES estimate for the momentum shift of 0.01 - 0.02 $Å^{-1}$ we obtain 3 - 6 meV, within range of the value extracted from Nakamura and Kimura's data.

3. Topological effects

A large number of perovskites has a simple cubic unit cell in a broad range of temperature, and whenever it is possible to cleave the crystal along the (111) plane, this results in a stacking of consecutive triangular sheets (see Figure 10). Di Xiao *et al.* [68] then proposed that by digitally growing bilayers of selected TMO perovskites along the (111) orientation one would engineer a graphene-like lattice where sites are occupied by the transition metal ion. The directional character of the t_{2g} and e_g bondings means that d-electron hoppings are essentially restricted to the bonds linking d-site neighbors. Main specificities of the TMO bilayers are the multi-orbital character of the carriers, values of the spin-orbit interaction ranging from small to large, confining potentials leading possibly to an electric field gradient across the layers, a polar charge on each layer. In addition, Coulomb interactions will play a decreasing role going from $3d$ to $5d$ elements. For an hexagonal lattice, Fu and Kane [69] showed that the parity operator for

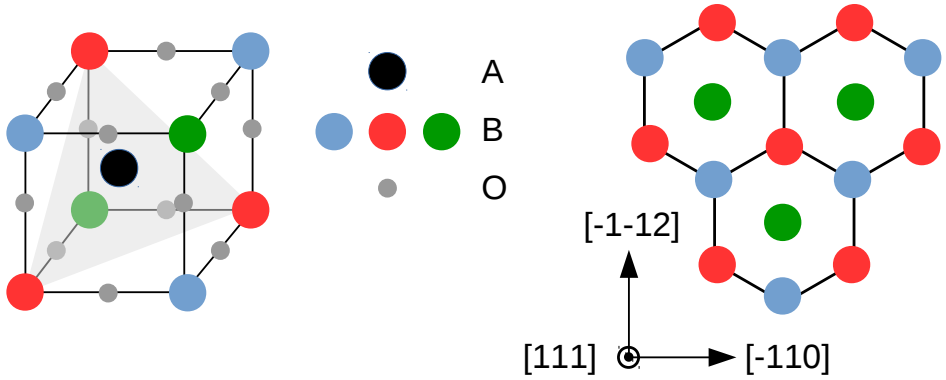

Figure 10. Unit cell of the cubic ABO_3 perovskite lattice with the (111) plane in gray. The red, green and blue dots are B cations in different (111) planes. Seen along the [111] direction, the B cations form a honeycomb lattice. Adapted with permission from T. Rödel *et al.*, Phys. Rev. Appl. **1**, 051002 (2014). Copyright (2014) by the American Physical Society.

the Time Reversal Invariant Momenta has the eigenvalue -1, implying a Z_2 topological phase for particular fillings. The parity symmetry of the electronic wavefunctions at the M points is reversed to that at Γ for some of the bands. Electric fields, Coulomb interactions and spin-orbit produce gaps across the Brillouin zone (BZ) allowing then for the formation of edge states in the topological insulating regime [70, 71, 72]. Aside from the above scenario, it was argued that for specific crystalline symmetries, in the case of bilayers sandwiched between large band gap insulators or superlattices, multiband-crossings occur and that through tuning the position of the Fermi energy to these points and taking into consideration electron-electron interactions one could stabilize topological regimes [73, 74, 75] (see Figure 11). An unusual topological state was theoretically proposed for bilayers of $SrRuO_3$ grown along the (111) direction. Based on DFT+DMFT calculations, Liang Si *et al.* [76] argued that due to the presence of a spin-orbit term, at 3/4 filling of the t_{2g} shell, a topological edge state can be promoted in the minority spin bands in coexistence with a half metallic, strongly ferromagnetic state. In order to reach the required value of the band fillings the authors suggest to replace Ru with Rh. On the experimental side, Santander *et al.* [77] proposed that the 2DEL observed at the bare surface of $KTaO_3$ grown along the (111) orientation [78] or of $SrTiO_3$ (111) [79] would host topological edge states. Key elements promote this feature. One is a high value of the confining electric field due to a stronger polar discontinuity at the surface than for the (001) orientation ($5e$ versus e for $KTaO_3$, $4e$ versus zero for $SrTiO_3$). Comparison between the data extracted from ARPES spectra and theory suggests indeed that modeling the bands using a bilayer tight binding hamiltonian is a fair approximation to the actual electronic structure for the $n_{2D} \sim 10^{14}$ cm^{-2} carrier concentrations that have been reported. The other factor is the bulk spin-orbit energy which gives rise to gaps across the BZ, as argued by Fu and Kane [69]. In both cases, however, the value of the filling factor implies that E_F lies several eV below the band

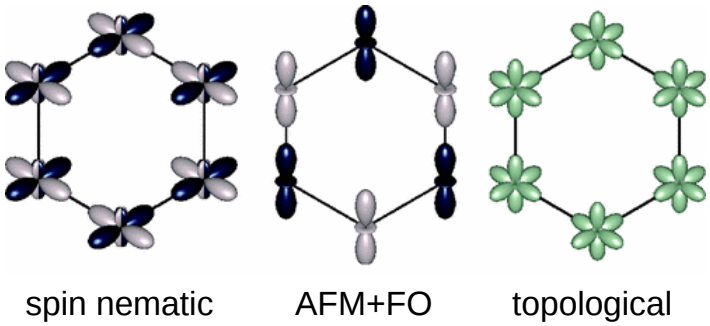

Figure 11. Spin and orbital ordered phases in AB'O_3/ABO_3/AB'O_3 heterostructures grown in the (111) direction. Considering e_g orbitals for the TM ions, several ordered phases can occur depending on the strength of the Coulomb repulsion U and the Hund coupling J: the illustration is for a spin nematic phase (bright and dark orbitals denote opposite majority-spin densities), antiferromagnetic (AFM) with ferro-orbital order (FO) and a topological phase. Reprinted with permission from A. Rüegg and G. Fiete, Phys. Rev. B **84**, 201103 (2011). Copyright (2011) by the American Physical Society.

gaps at the M points and this fact rules out the possibility of doping it with a gate in order to bring the two in coincidence.

The above discussion of a topological regime hinged on a parity inversion occurring at the M points of the BZ. An alternative way of generating such state is by driving the perovskite through a band inversion and this may happen when growing the TMO along the standard (001) orientation (see Figure 12). Tuning the spin-orbit interaction to open up a gap in the case of quadratic band crossings is one way to achieve this goal [80]. Substituting a chalcogene (Se, Te) or a halgene (Br, I) for Ti or Nb ions at the octaedral site of a cubic perovskite is a way to promote a large band inversion and the carrier concentration allowing one to produce a Z_2 topological regime. The bulk spin-orbit is required to open up a gap at E_F. In addition, a moderate amount of pressure needs to be applied to the material in order to counteract a spontaneous distorsion towards a non-cubic structure, caused by the substitution [81].

Lastly, the theoretical study of Vivek *et al.* [82] highlighted the existence of topological edge state at the 1D boundary of the 2D electron liquid seen at the (001) surface of $SrTiO_3$. The authors introduced a tight-binding modeling of the ARPES spectra featuring kinetic terms for the t_{2g} orbitals, sub-bands arising from the confinement of the 2DEG, bulk spin-orbit and an orbital mixing hybridization between the d_{xy} and $d_{xz/yz}$ states stemming from bond distortions at the surface. They found that at generic symmetry related points in the BZ a band inversion took place leading to a topological metallic state (see Figure 13). This state can easily be obtained by back-gating the sample since the position of E_F is only 3 meV above the gap. Chung *et al.* [83] suggested that at low enough temperature, a weak topological superconducting state would result and that it could be detected in STM experiments through the presence of majorana modes at edge dislocations. So far, the claims of topological states in oxide

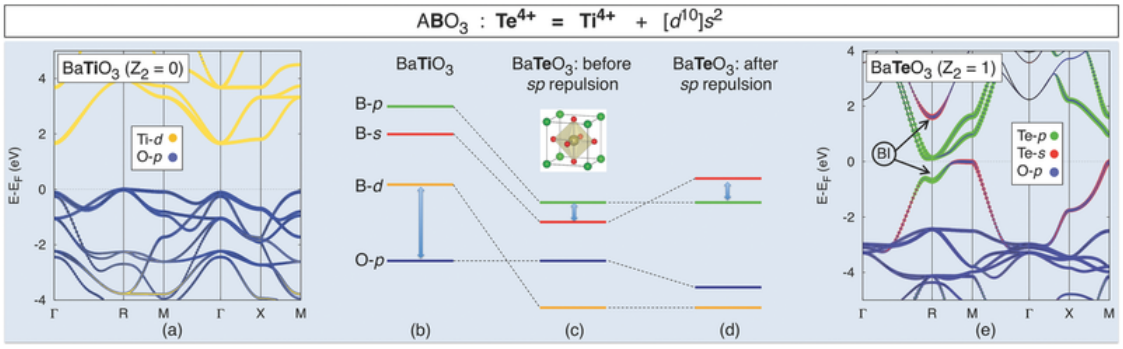

Figure 12. Concept of band inversion according to DFT calculations. (a),(b) The electronic structure of the band insulator (Z_2=0) $BaTiO_3$ shows a gap between O-2p states and Ti-3d states (blue arrow); (c) replacing Ti with Te, the gap opens within the Te states, between the 5s and the 4p bands; (d),(e) considering the effect of sp repulsion, there is a band inversion (BI) and the formation of a topological insulator (Z_2=1). This electronic structure is however strongly susceptible to atomic distortions that modify the cubic phase and suppress the band inversion. Reprinted from Ref. [81].

perovskites have been theoretical and experiments are definitely required to support their existence.

4. Conclusions

We have shown that spin-orbit coupling has been considered in the past decade as an important ingredient of the low-energy physics of 3d transition metal oxide surfaces and interfaces. Many exciting theoretical scenarios remain to be experimentally confirmed, such as the possibility of topological superconductivity and non-collinear magnetism [49, 84] at interfaces of $SrTiO_3$. An important area of investigation in the future is the physics of spin-orbit coupling at 5d transition metal oxides interfaces or at p-type interfaces [85]. Initial studies of 3d-5d and 4d-5d interfaces have focused on phenomena such as charge transfer and magnetic reconstructions [86, 87] as well as non-collinear magnetism [88]. Thanks to these new developments, spin-orbit coupling effects will remain firmly on the roadmap of oxide electronics in the years to come.

Acknowledgments

S. G. and J.-M. T. acknowledge the support of the Swiss National Science Foundation through Division II and of the European Research Council under the European Union's Seventh Framework Program (FP7/2007-2013)/ERC Grant Agreement No. 319286 (Q-MAC). A.C. acknowledges support by The Netherlands Organisation for Scientific Research (NWO/OCW) as part of the Frontiers of Nanoscience program (NanoFront), by the Dutch Foundation for Fundamental Research on Matter (FOM) and by the European Research Council under the European Union's H2020 Program/ERC Grant Agreement No. 677458.

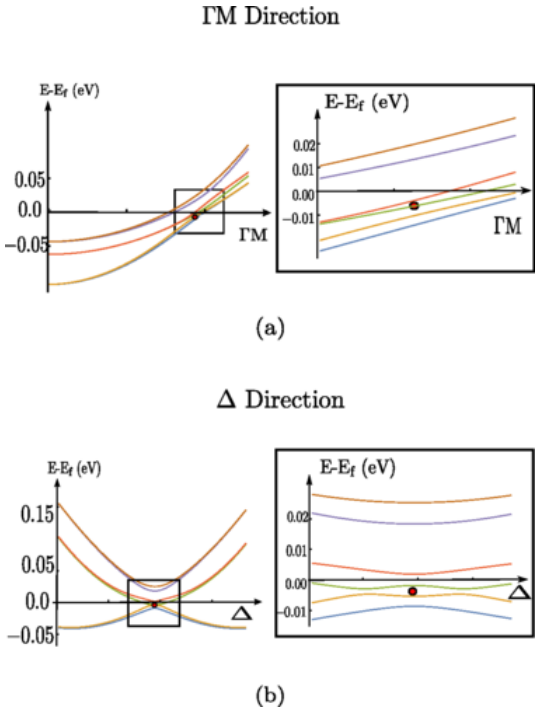

Figure 13. Band structure resolved in spin of $SrTiO_3$ surface showing two subbands with light mass and one band with heavy mass. The cuts are taken in the first quadrant of the BZ, along the ΓM direction (a) and the Δ direction (b) which is perpendicular to ΓM and passes through the avoided crossing (red dot). The spin-orbit interaction mixes the orbital terms at the avoided crossing and induces a band inversion which is visible along Δ but not along ΓM. Reprinted with permission from M. Vivek *et al.*, Phys. Rev. B **95**, 165117 (2017). Copyright (2017) by the American Physical Society.

References

[1] Sakurai J 1994 *Modern quantum mechanics* (Addison-Wesley)
[2] Shanavas K V, Popović Z S and Satpathy S 2014 *Phys. Rev. B* **90** 165108 URL http://link.aps.org/doi/10.1103/PhysRevB.90.165108
[3] Slater J 1960 *Quantum Theory of Atomic Structure* vol 2 (New York: McGraw-Hill)
[4] Herman F and Skillman S 1963 *Atomic Structure Calculations* (Englewood Cliffs, NJ: Prentice-Hall)
[5] Winkler R 2003 *Spin–Orbit Coupling Effects in Two-Dimensional Electron and Hole Systems* (Berlin, Heidelberg: Springer) ISBN 978-3-540-01187-3
[6] Pesin D and Balents L 2010 *Nat. Phys.* **6** 376–381 URL http://www.nature.com/doifinder/10.1038/nphys1606
[7] Witczak-Krempa W, Chen G, Kim Y B and Balents L 2014 *Annu. Rev. Condens. Matter Phys.* **5** 57–82 URL http://www.annualreviews.org/doi/abs/10.1146/annurev-conmatphys-020911-125138
[8] Rau J G, Lee E K H and Kee H Y 2016 *Annu. Rev. Condens. Matter Phys.* **7** 195–221 URL http://dx.doi.org/10.1146/annurev-conmatphys-031115-011319
[9] Hao L, Meyers D, Dean M P M and Liu J 2017 *ArXiv* 1711.07609 URL https://arxiv.org/abs/1711.07609
[10] Dresselhaus G 1955 *Phys. Rev.* **100** 580–586 URL http://link.aps.org/doi/10.1103/PhysRev.100.580

[11] Kane E 1957 *J. Phys. Chem. Solids* **1** 249–261
[12] Ohkawa F J and Uemura Y 1974 *J Phys. Soc. Jpn.* **37** 1325–1333
[13] Bychkov Y A and Rashba E I 1984 *JETP Lett.* **39** 78
[14] Edelstein V M 1990 *Solid State Commun.* **73** 233–235
[15] Zutic I, Fabian J and Sarma S D 2004 *Rev. Mod. Phys.* **76** 323
[16] LaShell S, McDougall B A and Jensen E 1996 *Phys. Rev. Lett.* **77** 3419–3422 URL https://link.aps.org/doi/10.1103/PhysRevLett.77.3419
[17] Ishizaka K, Bahramy M S, Murakawa H, Sakano M, Shimojima T, Sonobe T, Koizumi K, Shin S, Miyahara H, Kimura A, Miyamoto K, Okuda T, Namatame H, Taniguchi M, Arita R, Nagaosa N, Kobayashi K, Murakami Y, Kumai R, Kaneko Y, Onose Y and Tokura Y 2011 *Nat. Mater.* **10** 521–526
[18] Soumyanarayanan A, Reyren N, Fert A and Panagopoulos C 2016 *Nature* **539** 509–517
[19] Manchon A, Koo H C, Nitta J, Frolov S M and Duine R A 2015 *Nat. Mater.* **14** 871–882 URL http://dx.doi.org/10.1038/nmat4360%7B%25%7D5Cn10.1038/nmat4360
[20] Müller K and Burkard H 1979 *Phys. Rev. B* **19** 3593–3602 URL http://link.aps.org/doi/10.1103/PhysRevB.19.3593
[21] Itoh M, Wang R, Inaguma Y, Yamaguchi T, Shan Y j and Nakamura T 1999 *Phys. Rev. Lett.* **82** 3540
[22] Bednorz J and Müller K 1984 *Phys. Rev. Lett.* **52** 2289–2292 URL http://link.aps.org/doi/10.1103/PhysRevLett.52.2289
[23] Schooley J, Hosler W R and Cohen M L 1964 *Phys. Rev. Lett.* **12** 474
[24] Mattheiss L F 1972 *Phys. Rev. B* **6** 4740 URL http://link.aps.org/abstract/PRB/v6/p4740
[25] van der Marel D, van Mechelen J L M and Mazin I I 2011 *Phys. Rev. B* **84** 205111 URL http://link.aps.org/doi/10.1103/PhysRevB.84.205111
[26] El-Mellouhi F, Brothers E N, Lucero M J, Bulik I W and Scuseria G E 2013 *Phys. Rev. B* **87** 035107 URL https://link.aps.org/doi/10.1103/PhysRevB.87.035107
[27] Bistritzer R, Khalsa G and MacDonald A H 2011 *Phys. Rev. B* **83** 115114 URL http://link.aps.org/doi/10.1103/PhysRevB.83.115114
[28] Allen S J, Jalan B, Lee S, Ouellette D G, Khalsa G, Jaroszynski J, Stemmer S and MacDonald A H 2013 *Phys. Rev. B* **88** 045114 URL http://link.aps.org/doi/10.1103/PhysRevB.88.045114
[29] Uwe H, Yoshizaki R, Sakudo T, Izumi A and Uzumaki T 1985 *Jpn. J. Appl. Phys.* **24S2** 335–337 URL http://jjap.ipap.jp/link?JJAPS/24S2/335/
[30] Uwe H, Sakudo T and Yamaguchi H 1985 *Jpn. J. Appl. Phys.* **24-S2** 519 URL http://stacks.iop.org/1347-4065/24/i=S2/a=519
[31] Ohtomo A and Hwang H Y 2004 *Nature* **427** 423–6 URL http://dx.doi.org/10.1038/nature02308
[32] Reyren N, Thiel S, Caviglia A D, Kourkoutis L F, Hammerl G, Richter C, Schneider C W, Kopp T, Rüetschi A S, Jaccard D, Gabay M, Muller D A, Triscone J M and Mannhart J 2007 *Science* **317** 1196–9 URL http://www.sciencemag.org/cgi/content/abstract/317/5842/1196
[33] Gariglio S, Gabay M and Triscone J M 2016 *APL Mater.* **4** 060701 URL http://scitation.aip.org/content/aip/journal/aplmater/4/6/10.1063/1.4953822
[34] Pai Y Y, Tylan-Tyler A, Irvin P and Levy J 2018 *Rep. Progr. Phys.* **81** 036503 URL http://stacks.iop.org/0034-4885/81/i=3/a=036503
[35] Ben Shalom M, Sachs M, Rakhmilevitch D, Palevski A and Dagan Y 2010 *Phys. Rev. Lett.* **104** 126802 URL http://link.aps.org/doi/10.1103/PhysRevLett.104.126802
[36] Caviglia A D, Gabay M, Gariglio S, Reyren N, Cancellieri C and Triscone J M 2010 *Phys. Rev. Lett.* **104** 126803 URL http://link.aps.org/doi/10.1103/PhysRevLett.104.126803
[37] Elliott R J 1954 *Phys. Rev.* **96** 266–279 URL https://link.aps.org/doi/10.1103/PhysRev.96.266
[38] Yafet Y 1963 *Solid State Physics* **14** 1 – 98 URL http://www.sciencedirect.com/science/article/pii/S0081194708
[39] D'yakonov M I and Perel' V I 1972 *Sov. Phys. Solid State* **13** 3023
[40] Joshua A, Pecker S, Ruhman J, Altman E and Ilani S 2012 *Nat. Commun.* **3** 1129 URL

http://www.nature.com/ncomms/journal/v3/n10/full/ncomms2116.html
[41] Diez M, Monteiro a, Mattoni G, Cobanera E, Hyart T, Mulazimoglu E, Bovenzi N, Beenakker C W J and Caviglia A D 2015 *Phys. Rev. Lett.* **115** 016803
[42] Bovenzi N and Diez M 2017 *Phys. Rev. B* **95** 205430
[43] Nakamura H, Koga T and Kimura T 2012 *Phys. Rev. Lett.* **108** 206601 URL http://link.aps.org/doi/10.1103/PhysRevLett.108.206601
[44] Lesne E, Fu Y, Oyarzun S, Rojas-Sánchez J C, Vaz D C, Naganuma H, Sicoli G, Attané J P, Jamet M, Jacquet E, George J M, Barthélémy A, Jaffrès H, Fert A, Bibes M and Vila L 2016 *Nat. Mater.* **15** 1261–1266 URL http://www.nature.com/doifinder/10.1038/nmat4726
[45] Chauleau J Y, Boselli M, Gariglio S, Weil R, de Loubens G, Triscone J M and Viret M 2016 *Europhys. Lett.* **116** 17006 URL http://dx.doi.org/10.1209/0295-5075/116/17006
[46] Zhong Z, Tóth A and Held K 2013 *Phys. Rev. B* **87** 161102 URL http://link.aps.org/doi/10.1103/PhysRevB.87.161102
[47] Khalsa G, Lee B and Macdonald a H 2013 *Phys. Rev. B* **88** 041302
[48] Yada K, Onari S, Tanaka Y and Inoue J i 2009 *Phys. Rev. B* **80** 140509 URL http://link.aps.org/doi/10.1103/PhysRevB.80.140509
[49] Scheurer M S and Schmalian J 2015 *Nat. Commun.* **6** 6005 URL http://www.nature.com/doifinder/10.1038/ncomms7005
[50] Scheurer M S, Hoyer M and Schmalian J 2015 *Phys. Rev. B* **92** 014518 URL http://link.aps.org/doi/10.1103/PhysRevB.92.014518
[51] Santander-Syro A F, Copie O, Kondo T, Fortuna F, Pailhès S, Weht R, Qiu X G, Bertran F, Nicolaou A, Taleb-Ibrahimi A, Le Fèvre P, Herranz G, Bibes M, Reyren N, Apertet Y, Lecoeur P, Barthélémy A and Rozenberg M J 2011 *Nature* **469** 189–93 URL http://www.nature.com/doifinder/10.1038/nature09720
[52] Meevasana W, King P D C, He R H, Mo S K, Hashimoto M, Tamai A, Songsiriritthigul P, Baumberger F and Shen Z X 2011 *Nat. Mater.* **10** 114–8
[53] Santander-Syro A F, Fortuna F, Bareille C, Rödel T C, Landolt G, Plumb N C, Dil J H and Radović M 2014 *Nat. Mater.* **13** 1085–1090 URL http://www.nature.com/nmat/journal/v13/n12/full/nmat4107.html
[54] King P D C, McKeown Walker S, Tamai A, de la Torre A, Eknapakul T, Buaphet P, Mo S K, Meevasana W, Bahramy M S and Baumberger F 2014 *Nat. Commun.* **5** 3414 URL https://www.nature.com/articles/ncomms4414
[55] McKeown Walker S, Riccò S, Bruno F Y, de la Torre A, Tamai A, Golias E, Varykhalov A, Marchenko D, Hoesch M, Bahramy M S, King P D C, Sánchez-Barriga J and Baumberger F 2016 *Phys. Rev. B* **93** 245143 URL http://link.aps.org/doi/10.1103/PhysRevB.93.245143
[56] Garcia-Castro A C, Vergniory M G, Bousquet E and Romero A H 2016 *Phys. Rev. B* **93** 045405 URL https://link.aps.org/doi/10.1103/PhysRevB.93.045405
[57] Altmeyer M, Jeschke H O, Hijano-Cubelos O, Martins C, Lechermann F, Koepernik K, Santander-Syro A F, Rozenberg M J, Valentí R and Gabay M 2016 *Phys. Rev. Lett.* **116** 157203 URL https://link.aps.org/doi/10.1103/PhysRevLett.116.157203
[58] Rödel T C, Fortuna F, Sengupta S, Frantzeskakis E, Févre P L, Bertran F, Mercey B, Matzen S, Agnus G, Maroutian T, Lecoeur P and Santander-Syro A F 2016 *Adv. Mater.* **28** 1976–1980 URL http://dx.doi.org/10.1002/adma.201505021
[59] Frantzeskakis E, Rödel T C, Fortuna F and Santander-Syro A F 2017 *J. Electron Spectrosc. Relat. Phenom.* **219** Supplement C, 16 – 28 URL http://www.sciencedirect.com/science/article/pii/S0368204816301426
[60] Schultz M and Klein L 2007 *Appl. Phys. Lett.* **91** 151104
[61] Ueno K, Nakamura S, Shimotani H, Ohtomo A, Kimura N, Nojima T, Aoki H, Iwasa Y and Kawasaki M 2008 *Nat. Mater.* **7** 855–8 URL http://dx.doi.org/10.1038/nmat2298
[62] Ueno K, Shimotani H, Iwasa Y and Kawasaki M 2010 *Appl. Phys. Lett.* **96** 252107 URL https://doi.org/10.1063/1.3457785

[63] Gallagher P, Lee M, Petach T A, Stanwyck S W, Williams J R, Watanabe K, Taniguchi T and Goldhaber-Gordon D 2015 *Nat. Commun.* **6** 6437 URL http://dx.doi.org/10.1038/ncomms7437

[64] Nakamura H and Kimura T 2009 *Phys. Rev. B* **80** 121308 URL http://link.aps.org/doi/10.1103/PhysRevB.80.121308

[65] King P, He R, Eknapakul T, Buaphet P, Mo S K, Kaneko Y, Harashima S, Hikita Y, Bahramy M, Bell C, Hussain Z, Tokura Y, Shen Z X, Hwang H, Baumberger F and Meevasana W 2012 *Phys. Rev. Lett.* **108** 117602 URL http://link.aps.org/doi/10.1103/PhysRevLett.108.117602

[66] Santander-Syro A F, Bareille C, Fortuna F, Copie O, Gabay M, Bertran F, Taleb-Ibrahimi A, Le Fèvre P, Herranz G, Reyren N, Bibes M, Barthélémy A, Lecoeur P, Guevara J and Rozenberg M J 2012 *Phys. Rev. B* **86** 121107 URL https://link.aps.org/doi/10.1103/PhysRevB.86.121107

[67] Shanavas K V and Satpathy S 2014 *Phys. Rev. Lett.* **112** 086802 URL http://link.aps.org/doi/10.1103/PhysRevLett.112.086802

[68] Xiao D, Zhu W, Ran Y, Nagaosa N and Okamoto S 2011 *Nat. Commun.* **2** 596 URL https://www.nature.com/articles/ncomms1602

[69] Fu L and Kane C L 2007 *Phys. Rev. B* **76** 045302 URL https://link.aps.org/doi/10.1103/PhysRevB.76.045302

[70] Ando Y and Fu L 2015 *Ann. Rev. Condens. Matter Phys.* **6** 361–381 URL https://doi.org/10.1146/annurev-conmatphys-031214-014501

[71] Ren Y, Qiao Z and Niu Q 2016 *Rep. Progr. Phys.* **79** 066501 URL http://stacks.iop.org/0034-4885/79/i=6/a=066501

[72] Okamoto S and Xiao D 2017 *ArXiv e-prints* (*Preprint* 1705.05683) URL http://adsabs.harvard.edu/abs/2017arXiv1705056830

[73] Rüegg A and Fiete G 2011 *Phys. Rev. B* **84** 201103 URL http://link.aps.org/doi/10.1103/PhysRevB.84.201103

[74] Doennig D, Pickett W E and Pentcheva R 2013 *Phys. Rev. Lett.* **111** 126804 URL https://link.aps.org/doi/10.1103/PhysRevLett.111.126804

[75] Okamoto S, Zhu W, Nomura Y, Arita R, Xiao D and Nagaosa N 2014 *Phys. Rev. B* **89** 195121 URL https://link.aps.org/doi/10.1103/PhysRevB.89.195121

[76] Si L, Janson O, Li G, Zhong Z, Liao Z, Koster G and Held K 2017 *Phys. Rev. Lett.* **119** 026402 URL https://link.aps.org/doi/10.1103/PhysRevLett.119.026402

[77] Bareille C, Fortuna F, Rödel T C, Bertran F, Gabay M, Cubelos O H, Taleb-Ibrahimi A, Le Fèvre P, Bibes M, Barthélémy A, Maroutian T, Lecoeur P, Rozenberg M J and Santander-Syro A F 2015 *Sci. Rep.* **4** 3586 URL http://www.nature.com/articles/srep03586

[78] McKeown Walker S, de la Torre A, Bruno F Y, Tamai A, Kim T K, Hoesch M, Shi M, Bahramy M S, King P D C and Baumberger F 2014 *Phys. Rev. Lett.* **113** 177601 URL https://link.aps.org/doi/10.1103/PhysRevLett.113.177601

[79] Rödel T C, Bareille C, Fortuna F, Baumier C, Bertran F, Le Fèvre P, Gabay M, Hijano Cubelos O, Rozenberg M J, Maroutian T, Lecoeur P and Santander-Syro A F 2014 *Phys. Rev. Appl.* **1** 051002 URL https://link.aps.org/doi/10.1103/PhysRevApplied.1.051002

[80] Zhang H, Huang H, Haule K and Vanderbilt D 2014 *Phys. Rev. B* **90** 165143 URL https://link.aps.org/doi/10.1103/PhysRevB.90.165143

[81] Zhang X, Abdalla L B, Liu Q and Zunger A 2017 *Adv. Funct. Mater.* **27** 1701266 URL http://dx.doi.org/10.1002/adfm.201701266

[82] Vivek M, Goerbig M O and Gabay M 2017 *Phys. Rev. B* **95** 165117 URL https://link.aps.org/doi/10.1103/PhysRevB.95.165117

[83] Chung S B, Chan C and Yao H 2016 *Scientific Reports* **6** 25184 URL http://dx.doi.org/10.1038/srep25184

[84] Banerjee S, Erten O and Randeria M 2013 *Nat. Phys.* **9** 626–630 URL http://www.nature.com/doifinder/10.1038/nphys2702

[85] Lee H, Campbell N, Lee J, Asel T J, Paudel T R, Zhou H, Lee J W, Noesges B, Seo J, Park B, Brillson L J, Oh S H, Tsymbal E Y, Rzchowski M S and Eom C B 2018 *Nat. Mater.* **17** 231–236 URL `http://www.nature.com/articles/s41563-017-0002-4`

[86] Okamoto S, Nichols J, Sohn C Kim S Y, Noh T W and Lee H N 2017 *Nano Lett.* **17** 2126–2130

[87] Nichols J, Gao X, Lee S, Meyer T L, Freeland J W, Lauter V, Yi D, Liu J, Haskel D, Petrie J R, Guo E J, Herklotz A, Lee D, Ward T Z, Eres G, Fitzsimmons M R and Lee H N 2016 *Nat. Commun.* **7** 12721

[88] Matsuno J, Ogawa N, Yasuda K, Kagawa F, Koshibae W, Nagaosa N, Tokura Y and Kawasaki M 2016 *Science Advances* **2** e1600304